ACKNOWLEDGMENT

The authors are indebted to Dr. Mihai Elian and Dr. Kalman Ondrejcsik for valuable advice.

NOTATION

h = film thickness, mm.
Q = flow-rate, cc./sec.
r = distance along the film radius
R = film radius, mm.
v = radial velocity, mm./sec.
$\sigma_{12}, \sigma_{13}, \sigma_{23}$ = interfacial tensions (see Figure 7)
$\theta, \theta', \theta''$ = angles as shown in Figure 7; $\theta = \theta' + \theta''$

LITERATURE CITED

1. Suciu, D. G., Octavian Smigelschi, and Eli Ruckenstein, *AIChE J.*, 13, 1120 (1967).
2. ———, D. Eng. thesis, Polytechnical Inst., Bucharest, Romania (1968).
3. Fuchs, V. N., *Koll. Zeit.*, 52, 262 (1930).
4. Scriven, L. E., and Sternling C. V., *Nature*, 187, 186 (1960).

Manuscript received December 26, 1967; revision received April 15, 1968; paper accepted May 13, 1968.

Prediction of Jet Length in Immiscible Liquid Systems

BERNARD J. MEISTER and GEORGE F. SCHEELE

Cornell University, Ithaca, New York

The stability theory is used to predict jet length from jet inception to disruption for injection of one Newtonian liquid into a second immiscible Newtonian liquid. Knowledge of the length is essential for predicting the size of drops formed from jets. At low velocities jet length is controlled by the amplification of symmetrical waves which travel at the interfacial velocity of the jet. At higher velocities an abrupt lengthening of the jet may occur as a result of drop merging, and the jet length is then controlled by the growth rate of sinuous waves which are strongly velocity dependent. Jet disruption results from a geometrical limitation on the maximum amplitude of the sinuous waves. Predictions show good quantitative agreement with experimental data for thirteen mutually saturated systems over a wide range of variables and qualitative agreement with limited experimental data on the effects of initial disturbance level and mass transfer.

When a jet of liquid issues from a nozzle into a second immiscible liquid, the jet attains a length characteristic of the nozzle, injection velocity and physical properties of the liquids. Knowledge of the jet length is important primarily for the prediction of the size of drops formed from jets.

Smith and Moss (*26*) were the first to critically investigate the length of jets. They studied the jetting of liquids into air and derived an equation to predict jet length in the region where the length increases linearly with nozzle velocity. By recognizing that the jet length, L, is the length required for a disturbance to amplify to the magnitude of the jet radius, they obtained the equation

$$L = \frac{U_N}{\alpha} \ln\left(\frac{a_N}{\xi_0}\right) \qquad (1)$$

where α is the growth rate and ξ_0 is the initial amplitude of the most unstable symmetrical disturbance. Equation (1) assumes that the velocity and diameter of the jet are constant and equal to the average nozzle velocity and diameter. Substitution of Rayleigh's equation for α for injection of an inviscid liquid jet into a gas (*21*), and treatment of the quantity a_N/ξ_0 as a constant yields

$$\frac{L}{D_N} = K' N_{We}^{1/2} \qquad (2a)$$

where D_N is the nozzle or orifice diameter.

The data of Smith and Moss, Merrington and Richardson (*17*), Tyler and Richardson (*29*), and Tyler and Watkin (*30*) for low viscosity jets in air satisfy Equation (*2a*), although the constant K' varies from 11 to 16 in the several studies. This is not unexpected because the initial disturbance amplitude is probably a function of the experimental apparatus. Merrington and Richardson found that K' increased with increasing jet viscosity to a value of 84 for a 1,000 centipoise glycerine jet in air. The disturbance growth rate becomes much smaller for very viscous liquids, as shown by Weber's analysis (*33*), and the apparently high value of the constant results from the use of the Rayleigh equation for α in Equation (*2a*). If Weber's analysis for α is used, Equation (1) becomes

$$\frac{L}{D_N} = K' (N_{We}^{1/2} + 3 N_{We}/N_{Re}) \qquad (2b)$$

The data of both Haenlein (*8*) and Merrington and Richardson for viscous liquids show good agreement with Equation (*2b*), with values of $\ln(a_N/\xi_0)$ corresponding to those found from Equation (*2a*) for low viscosity jets.

Several experimental investigations (*12, 15, 24, 25, 30*) of the length of liquid jets in immiscible liquid systems have been made, but agreement with Equation (1) is not necessarily good in the linear region even when the appropriate values for α given by Meister and Scheele (*16*) are employed.

In both liquid-gas and liquid-liquid systems, the jet length-nozzle velocity curve displays a maximum. In liquid-gas systems, this maximum is generally very sharp and is followed immediately by jet disruption, which is characterized by the appearance of random waves, a broad drop size distribution and a sharp decrease in jet length. If

Bernard J. Meister is with The Dow Chemical Company, Midland, Michigan.

Weber's analysis is extended to include the pressure effects of an inviscid atmosphere, a maximum is predicted in the jet length-velocity curve. However, the quantitative prediction of the velocity at which the maximum occurs is poor. Grant and Middleman (7) present an empirical correlation for this velocity, and they then use the result to modify Weber's theory to obtain a satisfactory prediction of the jet length-velocity relationship over the entire laminar jet region. A significant feature of the analysis is the treatment of a_N/ξ_0 as a variable function of the Ohnesorge number, rather than as a constant.

In liquid-liquid systems, the maximum is more gradual and jet disruption may occur at much higher velocities than the jet length maximum. Correlations have been presented to predict the velocity at which maximum jet length occurs (*5, 18, 29, 30*). These correlations are empirical and generally apply over limited ranges of system parameters. In liquid-liquid systems, the velocity of jet disruption is a more important parameter than the velocity at maximum jet length because the resultant broad drop size distribution and low surface area per volume of dispersed phase makes the jet disruption velocity the upper operating limit for spray towers.

The objective of this paper is to present improved theoretical predictions for characterizing jet behavior as a function of nozzle velocity from jet formation to the onset of jet disruption in immiscible liquid systems. Prediction of the velocity at which a jet first forms has been the subject of a previous paper (*22*).

EXPERIMENTAL APPARATUS

Experimental data in the jetting region were obtained photographically for fifteen liquid-liquid systems and five nozzle diameters. Details of the apparatus and fluid properties are discussed in a previous paper (*22*), so only a brief summary is included here. The dispersed phase was injected through a nozzle made of 4 ft. long stainless steel tubing into a rectangular tank containing the stationary continuous phase. Nozzle diameter was varied from 0.0813 to 0.688 cm. The large length to diameter ratios were used to minimize disturbances and to assure a parabolic velocity distribution at the nozzle outlet.

Jet lengths and disturbance wavelengths and propagation velocities were measured from both 35 mm. still photographs and 2,500 frames/sec. motion pictures. Injection velocities were measured by using calibrated rotameters. Dispersed phase density was varied from 0.683 to 0.986 g./cc., continuous phase density from 0.990 to 1.254 g./cc., dispersed phase viscosity from 0.39 to 121 centipoises, continuous phase viscosity from 0.96 to 515 centipoises, and interfacial tension from 1.8 to 45.4 dyne/cm. Thirteen of the liquid-liquid systems were mutually saturated and two were used to study the effects of mass transfer.

EXPERIMENTAL RESULTS

Typical jet length data for a mutually saturated system are shown in Figure 1 as a function of injection velocity and nozzle diameter for heptane injection into water. In the initial region the length increases linearly with velocity. There is then an abrupt lengthening of the jet to two or three times its previous size, an additional gradual increase in length to a maximum, and finally a gradual decrease to a critical velocity beyond which the length decreases rapidly with increasing velocity. For the illustrated system this characteristic behavior is displayed by all jets except the one injected through the largest diameter nozzle; in this case the jet does not undergo abrupt lengthening.

Figure 1 shows that characterization of the jet behavior as a function of nozzle velocity will require predictions of the jet length-nozzle velocity dependence at low injection velocities, the velocity at which abrupt lengthening occurs, and the velocity of jet disruption.

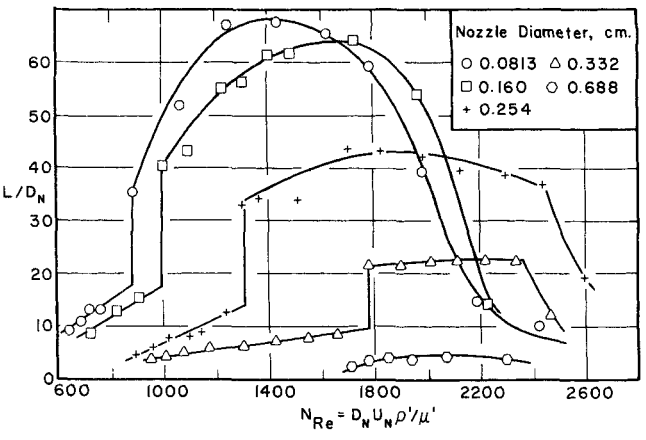

Fig. 1. Effect of nozzle diameter on dimensionless jet length for heptane injection into water.

JET LENGTH AT LOW INJECTION VELOCITIES

The validity of Equation (1) for liquid-gas systems suggests a similar approach should be valid for liquid-liquid systems. Of all the assumptions involved in Equation (1), the one most open to question in liquid-liquid systems at low injection velocities is that the disturbance wave transverses the jet at the average nozzle velocity. The celerity, or inherent velocity, of a symmetric wave whose amplitude is described by

$$\xi = \xi_0 \exp(at + ikz) \tag{3}$$

is given by

$$c = a/ik \tag{4}$$

Equation (4) shows that waves which have a real growth rate, a, and amplify with time have no real inherent velocity. Because the disturbance appears on the jet surface, the wave must therefore move at the velocity of the interface. For liquid jets in air, the gas phase offers negligible resistance, so within a short distance from the nozzle exit the velocity profile becomes flat and the interface velocity becomes equal to the average nozzle velocity if jet contraction is negligible. In liquid-liquid systems this is not the case.

If the interfacial velocity is not assumed to be equal to the nozzle velocity, the jet length equation has the more general form

$$\int_0^L \frac{dz}{U_I} = \frac{\ln(a_L/\xi_0)}{a} \tag{5}$$

when the dominant disturbance is a symmetrical wave of the form given by Equation (3) with a growth rate independent of velocity. At low injection velocities these assumptions are valid. The velocity dependence of the growth rate of symmetrical disturbances is considered in more detail in a later section of this paper and is shown to be small even at high injection velocities. Nonsymmetric waves with strong velocity dependent amplification rates do not become significant until the relative motion between dispersed and continuous phases becomes large.

It is known experimentally that the diameter of a jet contracts with increasing distance from the nozzle, and in the present study the maximum contraction observed was a 50% decrease in jet diameter. Meister (*15*) has shown that even this degree of contraction has little effect on jet length because of the compensating effects of an increase in jet velocity and an increase in the disturbance growth rate. This result agrees with the analysis of Ziabicki and Krozer (*34*). The additional assumption that the jet diameter is constant permits Equation (5) to be rewritten as

$$a_N^2 \int_0^L \frac{dz}{a^2 U_I} = \frac{\ln (a_N/\xi_0)}{\alpha} \tag{6}$$

where the ratio a^2/a_N^2 corrects the actual interfacial velocity to that which would exist in a noncontracting jet and α is evaluated for a jet of radius a_N.

Inherent in the derivation of Equations (5) and (6) is the assumption that a drop will break away from the jet when the dominant disturbance amplitude equals the jet radius. It will be shown in the next section that while this assumption is valid at low injection velocities, there is a critical nozzle velocity above which the hypothesis is incorrect.

Velocity Distribution in the Jet

To use Equation (6) it is necessary to be able to predict the interfacial velocity. Several velocity distributions have been proposed in the literature (*6, 31, 32*). Garner, Mina, and Jenson (*6*) derived a steady state velocity distribution by neglecting the inertial terms in the momentum equations. In most cases the jet breaks into droplets before the steady state distribution is attained, so this solution is not sufficient for the current problem. Vandegrift (*31*) obtained a velocity distribution for liquid-liquid jets by assuming a general form for the velocity distribution in each phase and evaluating the undetermined coefficients from boundary conditions. The solution does not appear applicable to the present study because it neglects interfacial tension forces and hence predicts jet widening in many cases rather than the contraction experimentally observed. Vandegrift's solution also considers a nonparabolic initial velocity distribution which is not appropriate for the present study.

Vrentas and Duda (*32*) have developed a numerical method for predicting the velocity distribution for liquid jets in gases. This method could be extended to liquid-liquid jets by employing a continuous phase shear stress at the interface, but this would not yield a mathematical expression for practical use.

Because of the objections to the previous solutions, it was necessary to derive a velocity distribution more suitable for the current problem. The approach taken parallels that of Vandegrift, with modifications to minimize the limitations inherent in such a solution. The velocity profile predicted by viscous forces is superimposed onto the tapered cylindrical shell obtained by considering the buoyancy and interfacial tension forces. The amplitude of the disturbances is considered small enough to have a negligible effect on the velocity profile.

The equations selected for the dispersed and continuous phases are, respectively,

$$\bar{U}_z' = \frac{1}{\bar{a}^2}\,[1 + \exp(-A\bar{z})]\left[1 - \frac{\bar{r}^2}{\bar{a}^2}\exp(-B\bar{z})\right] \tag{7}$$

$$\bar{U}_z = C \exp(-D\bar{r}^2) \tag{8}$$

where the velocities and distances are made dimensionless by the relations

$$\bar{U}_z = U_z/U_N;\ \bar{z} = 2\ z/D_N;\ \bar{a} = 2\ a/D_N;\ \bar{r} = 2\ r/D_N \tag{9}$$

and A, B, C, and D are independent of radial position $\bar{r}$ but are functions of axial distance $\bar{z}$.

The form of Equations (7) and (8) satisfies the following boundary conditions:

$$\text{At } \bar{z} = 0,\ \bar{U}_z' = 2(1 - \bar{r}^2) \tag{10a}$$

$$\text{At } \bar{z} = \infty,\ \bar{U}_z' = 1/\bar{a}^2 \tag{10b}$$

$$\text{At } \bar{r} = 0,\ \partial\bar{U}_z'/\partial\bar{r} = 0 \tag{10c}$$

$$\text{At } \bar{r} = \infty,\ \bar{U}_z = 0 \text{ and } \partial\bar{U}_z/\partial\bar{r} = 0 \tag{10d}$$

Five additional boundary conditions were selected to evaluate the four velocity profile constants and the jet radius as a function of axial distance. Continuity of axial velocity at the interface requires

$$(\bar{U}_z')_{\bar{r}=\bar{a}} = (\bar{U}_z)_{\bar{r}=\bar{a}} \tag{11}$$

The second boundary condition is continuity of shear stress at the interface. If the rate of jet contraction is sufficiently small that T_{rz} is the appropriate interfacial stress, this condition is

$$\mu'\left(\frac{\partial\bar{U}_z'}{\partial\bar{r}}\right)_{\bar{r}=\bar{a}} = \mu\left(\frac{\partial\bar{U}_z}{\partial\bar{r}}\right)_{\bar{r}=\bar{a}} \tag{12}$$

Continuity of mass in the jet is satisfied when

$$\int_0^{\bar{a}} \bar{U}_z'\,\bar{r}\,d\bar{r} = \frac{1}{2} \tag{13}$$

An overall momentum balance on the dispersed phase is the fourth boundary condition. If viscous forces are neglected, this condition becomes

$$2\rho'\,U_N^2\,\bar{U}_z'\frac{\partial\bar{U}_z'}{\partial\bar{z}} = g\Delta\rho D_N - \frac{8\sigma}{D_N}\frac{\partial(1/\bar{a})}{\partial\bar{z}} \tag{14}$$

Integration from $\bar{z} = 0$ to $\bar{z}$ yields

$$\bar{a}^4\left(g\Delta\rho D_N\bar{z} + \rho' U_N^2 + \frac{8\sigma}{D_N}\right) - \bar{a}^3\left(\frac{8\sigma}{D_N}\right) = \rho' U_N^2 \tag{15}$$

This equation is identical to Shiffler's jet contraction equation (*24*), it does not depend on the assumed velocity profile and superimposes the experimentally observed jet dimensions on the solution.

A number of boundary conditions could be selected as the fifth one. These include continuity of mass in the continuous phase and an overall momentum balance for the dispersed and continuous phases. These requirements are necessarily satisfied in an exact solution, but in a solution of the present type use of these continuous phase boundary conditions makes the dispersed phase velocity distribution strongly dependent on the assumed radial dependence of the continuous phase velocity because of the integration from the interface to infinity.

A more suitable equation is a momentum balance evaluated at either the interface or the center of the jet. As the interfacial velocity is the quantity of interest in this study, the momentum balance evaluated at the interface was selected as the fifth boundary condition. In this momentum balance, the interfacial tension and buoyancy terms included in Equation (14) were neglected. The second derivatives of the velocities in the axial direction,

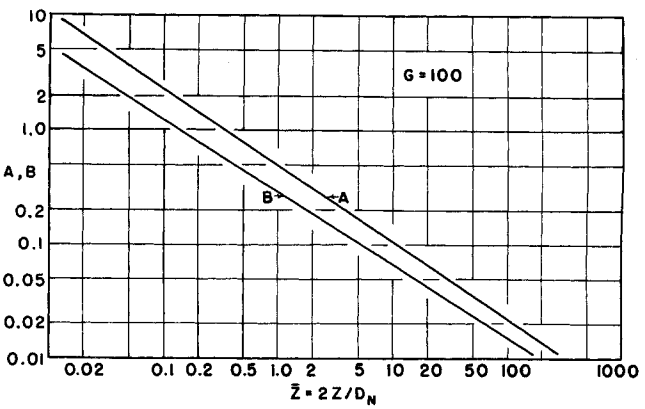

Fig. 2. Constants A and B in velocity profile analysis as a function of axial distance from the nozzle exit for a fluid with $G = 100$.

which are an order of magnitude less than the derivatives in the radial direction, were also neglected. Furthermore, in the various derivatives the jet radius was treated as a constant. Consistent with this assumption, the radial velocity terms in the momentum balance were neglected. The last two approximations could not be justified in a rigorous theoretical analysis but in a solution of the present type they simplify the equations significantly by uncoupling the boundary condition from Equation (15). Making the above simplifications, the fifth boundary condition becomes

$$\rho\bar{U}_z\frac{\partial\bar{U}_z}{\partial\bar{z}}-\rho'\bar{U}_z'\frac{\partial\bar{U}_z'}{\partial\bar{z}}=\frac{\mu}{U_Na_N}\left(\frac{\partial^2\bar{U}_z}{\partial\bar{r}^2}+\frac{1}{\bar{r}}\frac{\partial\bar{U}_z}{\partial\bar{r}}\right)-\frac{\mu'}{U_Na_N}\left(\frac{\partial^2\bar{U}_z'}{\partial\bar{r}^2}+\frac{1}{\bar{r}}\frac{\partial\bar{U}_z'}{\partial\bar{r}}\right) \quad (16)$$

evaluated at $\bar{r}=\bar{a}$.

Substitution of Equations (7) and (8) into Equations (11), (12), (13), and (16) and treatment of the jet diameter as a constant in differentiation yields the equations

$$[1+\exp(-A\bar{z})]\left[1-\frac{\exp(-B\bar{z})}{2}\right]=1.0 \quad (17)$$

$$\frac{\mu\Delta\rho U_Na_N[1-\exp(-B\bar{z})]^2\left\{\left[2B+2\bar{z}\frac{dB}{d\bar{z}}\right]-\left[A+\bar{z}\frac{dA}{d\bar{z}}\right][1-\exp(-B\bar{z})]\right\}}{\mu'^2[2-\exp(-B\bar{z})][\exp(-B\bar{z})]}=1.0 \quad (18)$$

Equations (17) and (18) can be solved quite readily for A and B as a function of $\bar{z}$ using the initial values calculated at the limit $\bar{z}=0$. The equations show that A and B are functions only of the group $G=a_NU_N\Delta\rho\mu/\mu'^2$ at a given value of $\bar{z}$. The limits of A and B as $\bar{z}\to 0$, obtained from Taylor series expansions of the exponentials, are

$$A=\left(\frac{3}{G}\right)^{1/3}\bar{z}^{-2/3} \quad (19a)$$

and

$$B=\left(\frac{1.5}{G}\right)^{1/3}\bar{z}^{-2/3} \quad (19b)$$

Figure 2 shows the solutions for A and B as a function of $\bar{z}$ for $G=100$. The slopes of A and B on a log-log plot are nearly constant over most of the range of interest.

When A and B have been determined, the ratio of the interfacial velocity to the average velocity can be calculated from the equation

$$\frac{U_I}{U_A}=[1+\exp(-A\bar{z})][1-\exp(-B\bar{z})] \quad (20)$$

The velocity ratio is a function only of G, and the computed results for values of G from 10^{-1} to 10^5 are shown

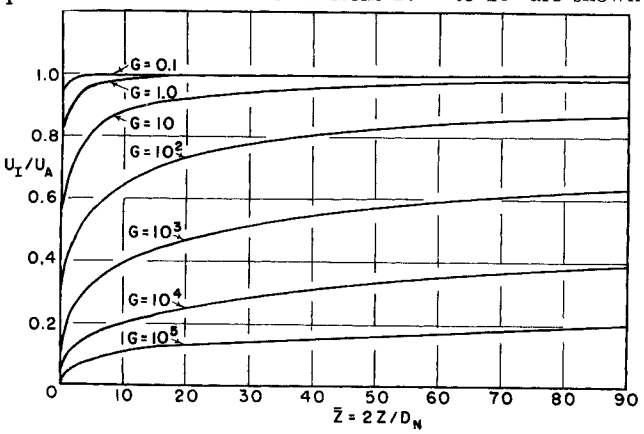

Fig. 3. Predicted interfacial velocity as a function of axial distance from the nozzle exit for several values of G.

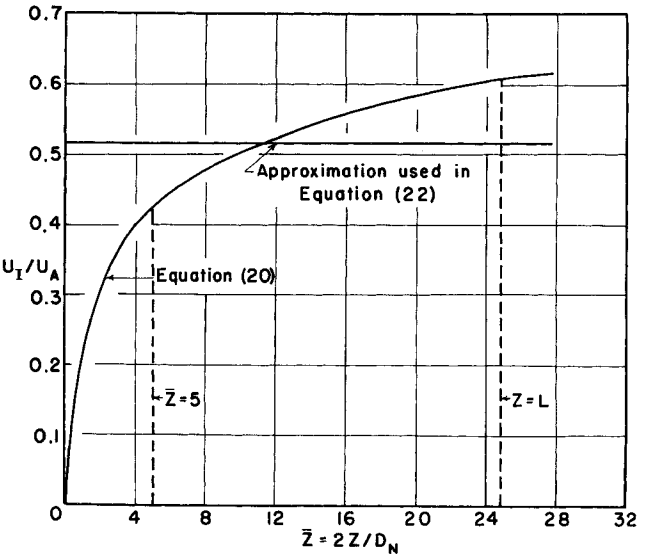

Fig. 4. Comparison of exact and approximate equations for interfacial velocity as a function of distance from nozzle exit for injection of heptane into water through 0.0813 cm. diameter nozzle. Injection velocity = 50 cm./sec.

in Figure 3. The interfacial velocity at any $\bar{z}$ can be calculated from the equation

$$U_I=(U_I/U_A)(U_N/\bar{a}^2) \quad (21)$$

by using Figure 3 to determine U_I/U_A and Equation (15) to calculate $\bar{a}$. The predicted interfacial velocities show good agreement with very limited experimental data obtained from high speed movies of heptane injection into water. The disturbance node velocities were measured in the region where the nodes were clearly visible and yet not large enough to distort the jet surface significantly. It was assumed that the node velocity is equal to the interfacial velocity. For $D_N=0.254$ cm., $U_N=20.0$ cm./sec. and $\bar{z}=10$, the predicted $\bar{U}_I$ of 0.855 compares favorably with the experimental value of 0.841. For $D_N=0.0813$ cm., $U_N=54.0$ cm./sec. and $\bar{z}=25$, the calculated and experimental values of $\bar{U}_I$ are 0.665 and 0.654, respectively.

The predicted values can also be compared to Vrentas and Duda's numerical solution for a water jet in air. The interfacial and centerline velocities predicted by the two methods are compared in Table 1 for the fluid properties $\mu=1.0$ centipoise, $\mu'=0.018$ centipoise, $\rho=1.0$ g./cc., and $\sigma=60$ dyne/cm. The interfacial velocities agree reasonably well. The centerline velocity agreement is not as good, particularly at low values of $\bar{z}$. This is expected because the present derivation was oriented towards prediction of the interfacial velocities.

TABLE 1. COMPARISON OF PREDICTIONS OF EQUATION (7) WITH NUMERICAL SOLUTION OF VRENTAS AND DUDA (32)

D_N, cm	U_N, cm./sec.	$\bar{z}$	$\bar{U}_I=U_I/U_N$ Equation (7)	$\bar{U}_I=U_I/U_N$ ref. 32	$\bar{U}_M=U_M/U_N$ Equation (7)	$\bar{U}_M=U_M/U_N$ ref. 32
0.222	41.9	5	1.25	1.15	1.67	2.15
0.222	41.9	10	1.65	1.55	1.91	2.25
0.222	41.9	20	2.04	2.05	2.25	2.45
0.222	41.9	40	2.71	2.75	2.82	2.90

Prediction of Jet Length

Equation (20) can be incorporated into Equation (6) to predict the jet length. The complex dependence of U_I on the axial distance from the nozzle precludes an analytical solution for jet length. Fortunately, the interfacial velocity does not change rapidly with distance from the nozzle exit after a sharp initial increase, so an arithmetic average of the interfacial velocities at $\bar{z} = 5$ and $z = L$ provides a satisfactory estimate of the interfacial velocity. Figure 4 compares this approximation with the theoretical interfacial velocity dependence on axial location for injection of heptane into water.

Using the approximate estimate of the interfacial velocity, Equation (6) can be expressed as

$$L = \frac{1}{2\alpha}\left[\left(\frac{a^2U_I}{a_N{}^2}\right)_{\bar{z}=5} + \left(\frac{a^2U_I}{a_N{}^2}\right)_{z=L}\right]\ln\left(\frac{a_N}{\xi_0}\right) \tag{22}$$

An iterative calculation is required to evaluate the interfacial velocity at the end of the jet because U_I is a function of L. Two iterations are generally adequate because U_I is not changing rapidly at $z = L$.

Equations (20) and (22) were used to predict the jet length-nozzle velocity dependence for the thirteen saturated liquid-liquid systems and five nozzle diameters used in this study. Values of α were obtained from the low velocity instability correlation of Meister and Scheele (*16*). The value of $\ln(a_N/\xi_0) = 6.0$ used for all calculations was evaluated both from the slope of the jet length curve at low velocities and, in the few instances where a large number of wave nodes were visible on the jet surface, by extrapolating the node amplitude back to the nozzle. Agreement of the two independent methods of calculation lends support to the value of 6.0 used.

While Equation (22) predicts a finite jet length for all injection velocities, there is a critical injection velocity below which a jet will not form. Scheele and Meister (*22*) have shown that this jetting velocity is given by the equation

$$U_J = 1.732\left[\frac{\sigma}{\rho' D_N}\left(1-\frac{D_N}{D_F}\right)\right]^{1/2} \tag{23}$$

Comparison of Theory with Experiment

Experimental jet lengths were obtained by averaging the measurements made from four photographs taken at each injection velocity. The total jet length measured included, in various stages of its formation, the drop about to break off from the jet. The jet length models assume that the jet ends when the amplitude of the disturbance equals the nozzle radius and so do not account for the added length of the forming drop which is included in any experimental measurement. To eliminate this discrepancy in comparing theory with experiment, an average value of the drop length was added to the theoretically predicted jet lengths.

Two of the experimental systems exhibited jet behavior characteristic of the large scale disturbance systems discussed in a later section of this paper. This behavior may have been due to the presence of a particle caught in the nozzle. For the other eleven mutually saturated systems, Equation (22) predicted jet length with a mean error of 24.0%. Use of the same values of α and $\ln(a_N/\xi_0)$ with Equation (1) gave a mean error of 90.6%. Although the error in using either Equation (1) or Equation (22) could be reduced by using a different value of $\ln(a_N/\xi_0)$ for each combination of system and nozzle, the node amplitude data indicated that the ratio was independent of system parameters in the present study.

The predictions of both equations were improved by use of α values obtained from the generalized correlation of Meister and Scheele (*16*). The additional improvement shown by Equation (22) arises from use of the interfacial velocity predicted by Equation (20) rather than the average nozzle velocity and is greatest for those systems having a highly viscous continuous phase and consequently a low interfacial velocity. The good agreement of theory with experiment substantiates the analysis leading to Equation (22).

The introduction of the interfacial velocity into the jet length equation makes it possible to explain why no jets are observed when heptane is injected into glycerine through large nozzles and when air is injected into liquids (*3, 10*). In these systems the interfacial velocity is so low that the most unstable disturbance amplifies to the nozzle radius within a short distance from the nozzle exit. For example, for the heptane-glycerine system and a 0.688 cm. diameter nozzle, the predicted length using Equation (22) is only 1.8 cm., whereas Equation (1) would predict a length of 18 cm. Therefore, although a force balance predicts jet formation (22), the appearance will still be that of drop formation. However, if the disturbance growth rate is independent of velocity, the drop formation time will become independent of velocity and the drops will form at a constant frequency independent of injection velocity rather than with the constant volume characteristic of drops formed at low injection velocities. This transition from constant drop volume to constant frequency of drop formation has been noted by most investigators when gases are injected into liquids.

CRITICAL VELOCITY FOR SHARP INCREASE IN JET LENGTH

An abrupt lengthening of the jet occurred at a particular nozzle velocity in almost all liquid-liquid systems studied. This phenomenon, shown in Figure 1 for heptane injection into water, has not generally been observed when liquids are injected into gases, and no prediction of its occurrence exists in the literature.

It is assumed in Equation (22) that when a disturbance on the jet surface reaches an amplitude equal to the jet radius, a drop is formed which escapes from the jet. The jet length is thus determined by the time for a disturbance to attain this amplitude. It is possible, however, that the drop formed will not have sufficient momentum to escape from the jet. In particular, if the drops are of uniform size and spherical, a detached drop must rise a distance of at least one drop diameter during the time of formation of the subsequent drop to escape from the jet. Although actual drops are deformed to some extent, the effects of deformation tend to cancel because the drop attached to the jet is elongated in the axial direction while the free drop is flattened due to drag resistance.

The analysis for predicting the abrupt lengthening of the jet due to drop merging is identical to that presented by Scheele and Meister (*22*) to predict jet formation arising from merging of drops at the nozzle exit. The condition for which a spherical drop will not separate from the jet is given by

$$\frac{D_F}{U_{Ri}} > \frac{V_F}{Q} \tag{24}$$

where U_{Ri} is the average rise velocity for the first diameter of rise. The nozzle velocity above which drop merging will occur is then

$$U_N = \frac{2\,D_F{}^2}{3\,D_N{}^2}\,U_{Ri} \tag{25}$$

Since no reliable equations exist for the unsteady state rise velocity, the empirical equations of Klee and Treybal (*13*) for the steady state rise velocity of drops were used to approximate U_{Ri} in Equation (25). Most studies of

the steady state rise velocity of drops (9, 11, 13) have shown that the rise velocity increases with drop diameter up to a critical diameter above which the velocity becomes independent of diameter. Klee and Treybal's equations for the two regions are

$$U_{R\infty} = 38.3\rho^{-0.45}\ \Delta\rho^{0.58}\ D_F^{0.70}\ \mu^{-0.11} \qquad (26)$$

for small drops, and

$$U_{R\infty} = 17.6\rho^{-0.55}\ \Delta\rho^{0.28}\ \sigma^{0.18}\ \mu^{0.10} \qquad (27)$$

for large drops. The critical diameter separating these two equations is

$$D_F = 0.33\rho^{-0.14}\ \Delta\rho^{-0.43}\ \sigma^{0.24}\ \mu^{0.30} \qquad (28)$$

The experimental Sauter average diameter at the nozzle velocity just prior to jet lengthening was used in calculations because drop size is not completely uniform in the jetting region.

The critical velocities predicted by Equation (25) were compared with the experimental velocities immediately before and after the abrupt jet lengthening occurred. These values are listed elsewhere (15). Predictions were in good agreement for most systems and the mean error was 13.4%. For several systems the merging process did not occur prior to jet disruption. If Equation (25) predicted a velocity higher than the velocity of jet disruption for these systems, the error was considered zero because the equation had successfully predicted the nonoccurrence of the phenomenon.

Predictions are not good for heptane injected into glycerine (system 3) and for a mixture of carbon tetrachloride and heptane injected into water (system 8). The errors can be attributed mainly to the use of the equations of Klee and Treybal to predict the rise velocity. These equations are not valid for a very viscous continuous phase, nor can an empirical equation be expected to predict the rise velocity for the very low density difference of 0.010 g./cc. used in system 8. These errors thus do not detract from the validity of the proposed mechanism for jet lengthening.

When the nozzle velocity exceeds the critical value predicted by Equation (25), an abrupt lengthening of the jet occurs. The jet lengthens until sinuous disturbances become large enough to throw the drop out of the path of the jet. The jet length can no longer be predicted by Equation (22) because, although the growth rate of the symmetric disturbances still controls drop size, it no longer controls the jet length. The sinuous waves which now control jet length are highly dependent on the relative velocity between the phases, so the relative phase velocities can no longer be ignored when jet lengthening occurs. A method of predicting jet length in this region is discussed in the next section.

CRITICAL VELOCITY FOR JET DISRUPTION

It is generally observed experimentally that there is a critical jet velocity above which the jet length decreases abruptly. Figure 1 illustrates this phenomenon for heptane injection into water. The sharp decrease in jet length is accompanied by a widening of the drop size distribution, so that for processes requiring small uniform size drops the jet disruption velocity determines the upper limit of operability.

Tyler and Richardson (29), Ohnesorge (18), and Grant and Middleman (7) have presented correlations for the jet disruption velocity for liquids injected into gases, and Fujinawa (5) and Tyler and Watkin (30) have correlated the critical velocity for liquids injected into liquids. The empiricism of these correlations makes it difficult to modify them for general applicability. In particular, the viscosity dependence of jet instability phenomena makes the extrapolation of correlations valid for limited physical property ranges uncertain. Because the breakdown must be associated with jet instability, it was decided to obtain a jet disruption criterion from stability analysis so that a better understanding of the mechanism of jet breakdown could be obtained.

At low injection velocities it has been shown that a stability analysis which considers only symmetrical waves with growth rates independent of velocity can predict jet instability. However, it is evident from Equation (6) that such an approach cannot predict the abrupt decrease in jet length observed at higher velocities. This suggests that the effect of the relative motion of the two phases on jet stability must be considered.

Inclusion of Relative Phase Motion in Jet Stability Analysis

Several instability analyses have been made which consider the relative motion of the jet and the continuous phase (4, 14, 20). Taylor (27) and Ranz and Dreier (20) have developed equations for instability at plane interfaces, and Ranz and Dreier have applied this approach to the prediction of drop formation from jets. Their solution is valid only at very high velocities where the disturbance wavelength is small compared to the jet diameter and drops are sheared from the surface of the jet.

Levich (14) has presented an approximate analysis for liquid jets in gases which treats the continuous phase as a perfect fluid. The solution predicts the experimentally observed increase in the growth rate and decrease in the wavelength of the dominant disturbance as the jet velocity increases.

Debye and Daen (4) derived an instability equation for inviscid liquid jets in an inviscid liquid. Their equation predicts that only symmetric disturbances are unstable at zero velocity, but that there is a critical nozzle velocity above which asymmetric disturbances become unstable. This velocity increases with increasing interfacial tension.

As the starting point for a more general stability theory, use is made of Tomotika's analysis (28), which is valid only when there is no relative motion of the phases. For symmetrical disturbances of the form given by Equation (3), Meister and Scheele (16) have summarized the limiting solutions and presented generalized correlations for wavelength and growth rate.

It is assumed that the disturbances can be represented by

$$\xi = \xi_0\ \cos(S\theta)\ \exp(\alpha t + ikz) \qquad (29)$$

where $S = 0$ corresponds to symmetrical disturbances which cause the jet to become varicose, $S = 1$ corresponds to asymmetric disturbances which cause sinuous motion of the jet, and higher values of S are not applicable to cylindrical jets. Tomotika's instability equation can be readily modified if motion in the angular direction is small compared with motion in the radial and axial directions. The only change in Tomotika's equation (33) is the replacement of the term $(1 - k^2a^2)$ by $(1 - k^2a^2 - S^2)$. The resulting equation can be represented in more convenient form as

$$\rho'\alpha^2(\ ) + \rho\alpha^2(\ ) + \mu'\alpha(\ ) + \mu\alpha(\ ) = \frac{\sigma(1 - k^2a^2 - S^2)ka(\ )}{a^3} \qquad (30)$$

where the empty parentheses are given in equation (C-72) of reference 15 and are functions of the wave number ka and the viscosity ratio μ'/μ. For $S = 1$, the right side of Equation (30) becomes negative for all positive values of ka. The empty parentheses are all positive, so the growth rate α must be negative or imaginary, indicating that all first-order waves are stable when the relative velocity is

zero.

Meister (*15*) incorporated the relative velocity into the analysis by superimposing a constant axial velocity on the perturbation equation for each phase and retaining in the momentum equation only those terms which were first-order in the perturbation. Use of these approximate velocity distributions does not satisfy the no-slip boundary condition at the jet surface which was assumed to be valid in the general analysis, but the more appropriate velocity distributions given by Equations (7) and (8) are too complex for this initial analysis. The resulting stability equation is

$$(\alpha - ikU_o')^2 \rho'(\ ) + (\alpha - ikU_o)^2 \rho(\ ) + (\alpha - ikU_o')\,\mu'(\ ) + (\alpha - ikU_o)\,\mu(\ ) = \frac{\sigma(1 - k^2a^2 - S^2)ka(\ )}{a^3} \quad (31)$$

where U_o' and U_o are the constant velocities of the dispersed and continuous phases, respectively, and the empty parentheses are the same as those in Equation (30).

Equation (31) is too complex to permit a general solution at this point. If both phases are inviscid, the dispersed and continuous phase velocities are U_N and 0, respectively, and Equation (31) reduces to

$$(\alpha - ikU_N)^2 \rho' \frac{I_0(ka)}{I_1(ka)} + \alpha^2 \rho \frac{K_0(ka)}{K_1(ka)} = \sigma \frac{(1 - k^2a^2 - S^2)ka}{a^3} \quad (32)$$

which, for S = 1, is identical to the equation derived by Debye and Daen (*4*).

For phases which are not inviscid, the choice of representative phase velocities must be more arbitrary. Since the objective of the present analysis is to account for the amplification of disturbances resulting from relative motion between the phases, the velocities chosen for U_o' and U_o were those which characterize the velocity gradient which most significantly affects the instability. For most systems the principal velocity gradient is in the dispersed phase, so the characteristic phase velocities U_o' and U_o selected are the average jet and interfacial velocities, respectively. When the dimensionless group G is less than 100, Equation (20) predicts that the principal velocity gradient is in the continuous phase so the characteristic phase velocities U_o' and U_o chosen are the average interfacial and continuous phase velocities. U_o is assumed to be zero for lack of a more satisfactory value. The following derivations are for the former case; similar equations could be derived for large ratios of dispersed to continuous phase viscosity.

Effect of Relative Velocity on Symmetrical Waves

In the derivation of Equation (22) the growth rate of the symmetrical waves has been assumed to be independent of velocity. This assumption can be checked using Equation (31). Meister and Scheele (*16*) have shown that, if both liquid viscosities are less than 1 centipoise, the viscous terms in the instability equation can be neglected. For S = 0, Equation (31) becomes

$$(\alpha - ikU_A)^2 \rho' \frac{I_0(ka)}{I_1(ka)} + (\alpha - ikU_I)^2 \rho \frac{K_0(ka)}{K_1(ka)} - \frac{\sigma(1 - k^2a^2)ka}{a^3} = 0 \quad (33)$$

where U_A and U_I are the average jet velocity and average interfacial velocity, respectively. The disturbance growth rate, obtained by rearranging Equation (33) and retaining only the real part, is given by

$$\alpha^2 = \frac{k^2 \rho' \rho I_{0k}K_{0k} (U_A - U_I)^2}{(\rho' I_{0k} + \rho K_{0k})^2} + \frac{\sigma(1 - k^2a^2)ka}{a^3 (\rho' I_{0k} + \rho K_{0k})} \quad (34)$$

where $I_{0k} = I_0(ka)/I_1(ka)$ and $K_{0k} = K_0(ka)/K_1(ka)$. If it is assumed that the Bessel function ratios are independent of k, the dominant wavelength is predicted to be

$$k_{max} = \frac{\rho' \rho I_{0k}K_{0k} (U_A - U_I)^2}{3\sigma (\rho' I_{0k} + \rho K_{0k})} + \left\{ \left[\frac{\rho' \rho I_{0k}K_{0k} (U_A - U_I)^2}{3\sigma (\rho' I_{0k} + \rho K_{0k})} \right]^2 + \frac{1}{3a^2} \right\}^{1/2} \quad (35)$$

Predicted values of α_{max} and $(ka)_{max}$ are compared in Table 2 with experimental results obtained for heptane injection into water through a 0.254 cm. diameter nozzle. The same averaging procedure as that in Equation (22) was used to calculate mean interfacial and average jet velocities. Values of U_I were calculated from Equation (20), and values of U_A were obtained by combining Equation (15) for jet contraction with the requirement of mass conservation. Experimental measurements of the wave number are not extremely accurate because some contraction has occurred by the time the wave becomes visible. Furthermore, the volume of fluid between wave nodes increases with time because of the velocity distribution in the jet. For these reasons the wave number was measured when the wave first became visible.

Table 2. Effect of Nozzle Velocity on Growth Rate and Wave Number of Symmetric Waves for Heptane Injection into Water through 0.254 cm. Diameter Nozzle

	ka		α, sec.$^{-1}$
U_N, cm./sec.	Experimental	Equation (35)	Equation (34)
19.9	0.68	0.625	56.4
29.6	0.70	0.690	60.0
38.6	0.75	0.788	67.5

Theoretical wave numbers show good agreement with experiment and lend support to the stability analysis. The analysis of Ranz and Dreier for liquid-liquid systems is not applicable because the disturbance wave length is larger than the jet radius. The predicted growth rate of the symmetrical disturbances increases only 20% over the velocity range of interest. Neglect of the effect of velocity on α in the jet length prediction at low injection velocities thus appears to be a satisfactory approximation for low viscosity liquids. No analysis has been made for high viscosity liquids because of the complexity of Equation (31), but one would expect the effect to be less at equal Weber numbers due to the viscous damping of the instability.

Effect of Relative Velocity on Sinuous Waves

Sinuous waves amplify only when there is relative motion of the two phases. The growth rate and wavelength of these waves can also be determined from Equation (31). For two low viscosity liquids, substitution of S = 1 and rearrangement yields

$$\alpha^2 = \frac{k^2 \rho' \rho I_{0k}K_{0k} (U_A - U_I)^2}{(\rho' I_{0k} + \rho K_{0k})^2} - \frac{k^3 \sigma}{(\rho' I_{0k} + \rho K_{0k})} \quad (36)$$

The wavelength which maximizes Equation (36) is a strong function of velocity, so the Bessel function ratios cannot be treated as constants. The growth rate and wave number of the most unstable wave must be evaluated numerically.

A comparison of experimental and theoretical wave

numbers is presented in Table 3 for heptane injection into water using a 0.254 cm. diameter nozzle. Agreement between the calculated and measured wavelengths is reasonably good, the maximum deviation being 30%. A strong velocity dependence is shown by both experiment and theory.

Table 3. Effect of Nozzle Velocity on Growth Rate and Wave Number of Sinuous Waves for Heptane Injection into Water through 0.254 cm. Diameter Nozzle

	ka		α, sec.$^{-1}$
U_N, cm./sec.	Experimental	Theoretical	Equation (36)
29.6	0.20	0.260	3.1
38.6	0.495	0.620	17.4
49.0	0.870	0.950	59.2

The growth rate of the sinuous disturbances can be used to estimate jet length in the region following the abrupt lengthening of the jet. At an injection velocity of 38.6 cm./sec., the growth rate of the sinuous disturbances is about ¼ that of the symmetric disturbances for the heptane-water system considered in Tables 2 and 3. At the same velocity the experimental jet length is about three times what it would be if symmetric disturbances controlled the jet length and Equation (22) were applicable. A hypothesis consistent with these results is that the initial amplitude of the sinuous waves is equal to that of the symmetrical waves, since both are probably initiated simultaneously by the same disturbance. When the amplitude of the sinuous disturbances attains the magnitude of the jet radius, the lateral motion of the jet is sufficiently large to throw the drops out of the path of the jet. Photographic evidence supports this hypothesis. The jet length can then be calculated from the time required for the amplitude of the sinuous waves to become equal to the jet radius.

Prediction of Jet Disruption Velocity

It can be shown geometrically that a sinuous wave with a wavelength, λ, on a jet of radius, a, cannot have an amplitude, ξ, greater than

$$\xi/a = 1/ka \tag{37}$$

It is hypothesized that jet disruption will occur at the lowest injection velocity for which ξ reaches the critical value given by Equation (37) prior to jet termination resulting from drop breakoff caused by the amplification of symmetrical disturbances.

For low disturbance systems where abrupt lengthening of the jet due to drop merging occurs before jet disruption, the amplitude of the sinuous waves at the end of the jet is approximately equal to the jet radius because, as discussed in the previous section, an amplitude close to this value is required to throw the drops away from the jet. If ξ is less than a, drops will not break off due to the amplification of symmetrical waves even though the growth rate is large enough to form drops. The critical value of ξ is thus the jet radius a, and Equation (37) predicts jet disruption will first occur at that injection velocity for which the dimensionless wave number, ka, for the sinuous waves equals 1.0. As the velocity is increased above the critical, the jet will shorten rapidly because of the increase in both growth rate and wave number of the dominant sinuous wave with increasing velocity. The increase in wave number decreases the maximum amplitude the sinuous waves can have.

There are also low disturbance systems where jet disruption occurs prior to drop merging. Sinuous waves will disrupt these jets if they reach the critical amplitude ξ before the symmetrical waves grow to an amplitude a. If the initial amplitudes of the symmetrical and sinuous waves are the same, an approximation supported by experimental evidence, the critical amplitude for the sinuous waves must be less than the jet radius, because the growth rate of the sinuous waves is always predicted to be less than that of the symmetrical waves. Consequently, ka of the sinuous waves that disrupt the jet must be greater than 1.0.

In the limit of large wave numbers, the growth rates of the most unstable symmetrical and sinuous waves approach one another. Extrapolation of the data in Tables 2 and 3 shows that, for heptane injection into water through a 0.254 cm. diameter nozzle, the growth rates are becoming quite close at a sinuous wave ka value of 1.0, so a value of ka only slightly greater than 1.0 is required for jet disruption. This result is quite general and is consistent with experimental data which showed that the amplitude of the sinuous waves at the end of the jet immediately prior to jet disruption was approximately equal to the jet radius and that the wave number of the dominant sinuous waves was approximately 1.0. Therefore, the criterion that $ka = 1.0$ for sinuous waves is sufficiently precise to predict jet disruption whether or not drop merging occurs. An equation can be obtained for the jet disruption velocity for injection of a low viscosity liquid into a low viscosity continuous phase when $G > 100$. If Equation (36) is differentiated with respect to k to determine k_{max} and if the resulting ka is set equal to 1.0, the critical velocity criterion becomes

$$(U_A - U_I)^2 = \frac{1.905\sigma\ (2.25\rho' + 0.70\rho)}{\rho'\ \rho D_N} \tag{38}$$

When the viscosities and densities of the two phases are equal, $U_A - U_I \approx U_N/\sqrt{2}$ and Equation (38) reduces to a constant Weber number criterion for jet disruption.

$$U_N \sqrt{\frac{\rho' D_N}{\sigma}} = 3.36 \tag{39}$$

This is consistent with the empirical correlations in the literature (*5, 18, 29, 30*), all of which involve the Weber number. Ranz (*19*) predicts that thrashing and nonuniform drop size begin when

$$U_N \sqrt{\frac{\rho D_N}{\sigma}} > 2.83.$$

The predictions of Equation (38) are compared in Table 4 with the velocity range within which jet disruption occurred experimentally. The system numbers correspond to those in Table 1 of reference 22. Equation (20) was employed to predict the average interfacial velocity used in the theoretical analysis. When the viscosity of each phase was less than 3.0 centipoises and G was greater than 100, the predicted velocity was within the experimental range.

The agreement between experiments and the low viscosity analysis supports the jet disruption hypothesis. For more viscous liquids it is not possible to obtain an analytical expression for the disruption velocity. Table 4 shows that Equation (38) gives a good estimate for systems with a large continuous phase viscosity, but the predictions are greatly in error when the velocity gradient is principally in the continuous phase, as for example when the dispersed phase is very viscous. For these systems the characteristic phase velocities U_o' and U_o can be better approximated as U_I and 0, respectively. The equation corresponding to Equation (38) is then

$$U_I^2 = \frac{1.905\sigma\ (2.25\rho' + 0.70\rho)}{\rho\ \rho' D_N} \tag{40}$$

TABLE 4. PREDICTION OF JET DISRUPTION VELOCITY

System	Nozzle Diameter, cm.	G	Viscosities, Centipoises μ	μ'	Experimental Range of Jet Disruption Velocity, cm./sec.	Theoretical Velocity, cm./sec.	
$G > 100$: both phase viscosities less than 3.0 centipoises							
						Equation (38)	
1	0.0813	936	0.958	0.393	112-125	118.0	
1	0.160	1,215	0.958	0.393	71.0-79.6	78.0	
1	0.254	1,475	0.958	0.393	59.0-62.5	59.5	
1	0.332	1,460	0.958	0.393	40.7-42.7	45.0	
1	0.688	1,770	0.958	0.393	22.4-29.4	26.5	
13	0.0813	190	0.958	0.544	106-117	115.5	
$G > 100$: continuous phase viscosity greater than 3.0 centipoises							
						Equation (38)	
2	0.0813	363,000	515	0.393	52.0-54.0	47.0	
3	0.0813	124,800	168	0.393	52.0-54.0	50.8	
4	0.0813	59,000	78.5	0.393	52.0-54.0	52.5	
5	0.0813	18,550	21.9	0.393	54.0-64.5	63.2	
5	0.254	27,400	21.9	0.393	31.4-33.0	29.9	
6	0.0813	5,650	6.95	0.393	54.0-64.5	67.5	
6	0.254	6,550	6.95	0.393	26.4-28.0	25.0	
$G < 100$							
						Equation (38)	Equation (40)
9	0.254	0.0047	0.958	121	greater than 42.8	15,700	35.2
10	0.254	0.0935	0.958	35.3	greater than 64.4	2,660	34.6
11	0.254	0.48	0.958	15.7	61.2-65.8	810	35.2
12	0.254	3.2	0.958	6.71	62.9-73.5	405	39.8
7	0.0813	5.7	1.09	2.52	50.4-55.2	87	10.1
7	0.160	4.9	1.09	2.52	20.9-25.4	45	3.0
8	0.0813	16.5	0.958	0.488	96.8-106	360	50.2
8	0.254	27.0	0.958	0.488	50.9-55.3	170	29.1

Table 4 indicates that this equation gives a much better estimate of the velocity of jet disruption for the systems with a large dispersed phase viscosity and illustrates the importance of having good estimates of the relative velocities for stability calculations. Satisfactory agreement is not obtained because of the neglect of the viscous terms in the instability equation. Neither equation gives very satisfactory predictions for systems 7 and 8 which have intermediate G values. Not surprisingly, the experimental values of jet disruption are between the predictions of Equations (38) and (40).

If the jet disruption velocity is lower than the critical nozzle velocity predicted by Equation (25) for drop merging, abrupt lengthening of the jet will not occur. This is illustrated by injection of heptane into glycerine (system 2) through a 0.0813 cm. diameter nozzle. In this system jet disruption occurred first. Theoretical predictions are consistent with this observation. The discontinuity in the jet length curve is predicted to occur for $U_N = 177.5$ cm./sec., while the theoretical jet disruption velocity given in Table 4 is 47.0 cm./sec.

EFFECTS OF INITIAL DISTURBANCE LEVEL AND MASS TRANSFER ON JET BEHAVIOR

The analysis and results presented in previous sections of this paper assume minimum disturbance conditions and consider mutually saturated liquid phases. In practice neither of these conditions may be met. Consequently, even though the major purpose of this study was an attempt to understand the idealized situation, initial experiments were performed to assess qualitatively the effects of large-scale initial disturbances and mass transfer on jet behavior.

Initial Disturbances Level

Prediction of the jet length in a practical situation is difficult because of lack of knowledge of the initial disturbance level. In commercial equipment, nozzle roughness and process disturbances are likely to cause initial disturbance amplitudes larger than the value $\xi_0 = a_N \exp(-6.0)$ found for the nozzles in this study.

To investigate the effects of the initial disturbance level, a 200 mesh stainless steel screen was inserted in a nozzle at varying distances from the nozzle exit. The jet length data for the artificially disturbed systems are compared with the data for the undisturbed system in Figure 5. At low injection velocities the existence of the artificial disturbances had little effect on the jet length. This is probably due to two compensating factors. The larger initial disturbance level should reduce the jet length if no other parameter changes. However, the large-scale eddies also produce a flatter velocity profile at the nozzle exit, and consequently the jet interfacial velocity is higher. These two effects counteract one another, as can be seen from Equation (22). It is also possible that, at low velocities, the eddies generated by the wire completely decayed by the time the liquid reached the nozzle exit. Whatever the explanation, it appears that at low injection velocities the jet length-nozzle velocity dependence observed in these experiments can be characterized satisfactorily by low disturbance experiments.

The major effect of an increase in the disturbance level was a decrease in the jet disruption velocity, as shown in Figure 5. In many systems disruption occurred at a velocity sufficiently low that the abrupt jet lengthening characteristic of many low disturbance systems did not occur. Quantitative prediction of the jet disruption velocity using

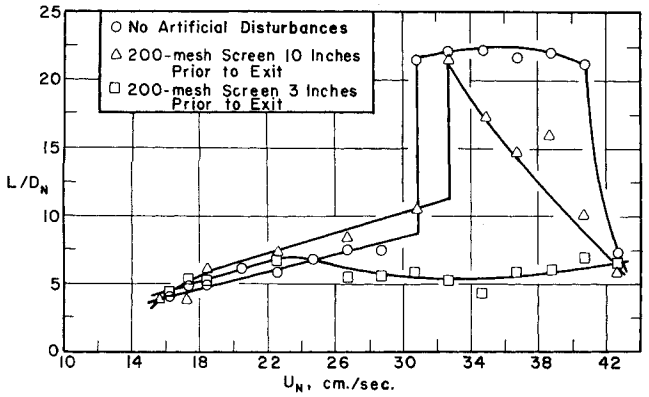

Fig. 5. Effect of artifical disturbances on dimensionless jet length for heptane injection into water through 0.332 cm. diameter nozzle.

the previously developed criterion cannot be made until the effects of the artificial disturbances are better characterized. In particular, it is necessary to know how the disturbances affect the initial amplitudes of the symmetrical and sinuous waves. It is apparent that initial amplitudes will increase with increasing disturbance level, but it is not known if the initial amplitudes of the two types of waves will remain approximately equal. It is also not known if the most unstable waves will be those predicted by stability analysis. The disturbance generators may selectively give such a high initial amplitude to a narrow band of waves that even though these waves do not have the highest growth rate they will cause jet instability.

The data suggest that in most real equipment the drop merging phenomenon may not occur. This indicates that a degree of caution is required in the use of laboratory data for the design of commercial equipment when instability phenomena are involved.

Mass Transfer

The effect of mass transfer was studied using the benzene-water system with 5.0% by weight acetone in the solute-rich phase. This system was chosen because the distribution coefficient of acetone between the benzene and water phases is approximately 1.0 on a weight percent basis for acetone concentrations below 10%. Thus the effect of the direction of mass transfer on jet length is not coupled with a driving force effect for a fixed acetone concentration in the solute-rich phase. The interfacial tension decreases from 31.2 to 20.2 dynes/cm. as the equilibrium acetone concentration increases to 5.0%. None of the other physical properties changes significantly.

Representative experimental jet lengths are illustrated in Figure 6. The data show that mass transfer decreased the initial jetting velocity, increased the jet length at a given nozzle velocity in the low velocity region, and decreased the jet disruption velocity. All of these effects are consistent with the lowering of the interfacial tension σ which accompanies addition of acetone to the system. Scheele and Meister (22) have shown that the jetting velocity is directly proportional to $\sigma^{1/2}$. For a low viscosity liquid jet injected into a low viscosity liquid, Christiansen (2) has shown that the growth rate of the most unstable disturbance is proportional to $\sigma^{1/2}$, a result which can be used with Equation (22) to predict that the jet length should decrease with $\sigma^{1/2}$. Equation (38) shows that as an approximation the jet disruption velocity is proportional to $\sigma^{1/2}$.

It has been noted by many investigators that mass transfer into a drop tends to stabilize the interface and deter coalescence, while mass transfer out of a drop tends to destabilize it and promote coalescence. One might expect the same phenomenon to occur in a jet. This effect is illustrated in Figure 6 where the system with mass transfer into the jet displays greater jet lengths than the corresponding system with mass transfer out of the jet.

SUMMARY

1. The characterization of jet behavior in liquid-liquid systems as a function of nozzle velocity from jet formation to the onset of jet disruption requires prediction of several phenomena.

2. The velocity at which a jet first forms can usually be predicted from a force balance at the nozzle exit. Prediction of this velocity was the subject of a previous paper (22). The jetting velocity is given by Equation (23) for a parabolic jet velocity distribution at the nozzle exit.

3. At low injection velocities, jet length can be predicted as a function of nozzle velocity from stability theory by determining the distance required for symmetrical disturbances to attain an amplitude equal to the jet radius. Knowledge of the initial disturbance level, which must be estimated from experimental data, is required. The interfacial velocity must also be known because the disturbances travel at this velocity. The interfacial velocity can be predicted from Equation (20) for the case where the initial jet velocity distribution is parabolic. The jet length can be predicted exactly from Equation (5), and Equation (22), which is easier to use, is a satisfactory approximation.

4. In the general stability analysis both symmetrical and sinuous disturbances must be considered. At low injection velocities the growth rates of the sinuous waves are zero or so low that only symmetrical disturbances need be considered. As the velocity increases the sinuous waves become increasingly significant. Because both the growth rate and wavelength of these sinuous waves are strongly velocity dependent, the velocity distributions in the jet and continuous phases must be incorporated into the stability analysis. Although this has been done only in an approximate fashion in the present analysis, the success of predictions based on the analysis suggests that the general approach is valid and that more rigorous stability calculations would be of value.

5. In low disturbance systems there is often a critical velocity at which the jet increases abruptly in length, The occurrence of this phenomenon, which results because the drops formed do not have sufficient rise velocity to escape from the jet, can be predicted by using Equation (25). Once the merging has occurred, jet length is controlled by the sinuous disturbances, which must grow to sufficient amplitude to throw the drops out of the path of the jet. It is estimated that the critical amplitude is equal to the jet radius. Drop size continues to be controlled by the symmetrical disturbances.

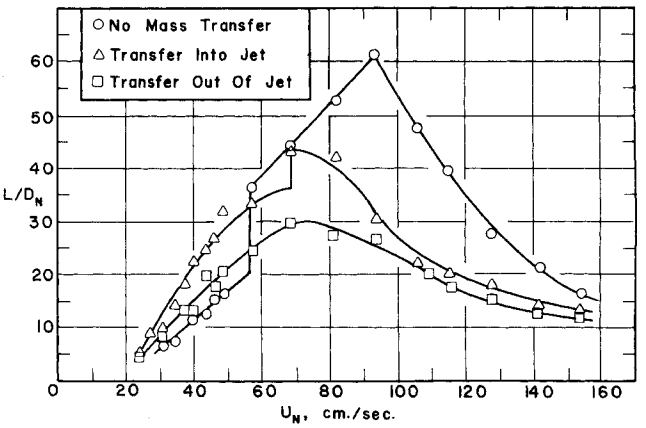

Fig. 6. Effect of mass transfer on dimensionless jet length for benzene injection into water with acetone the transferring solute. Nozzle diameter = 0.0813 cm.

6. There is a jet disruption velocity above which the jet length decreases sharply with increasing velocity and the drop formation process becomes erratic. This disruption is apparently due to the geometrical limitation on the maximum amplitude of the sinuous waves which is given by Equation (37). For low disturbance systems the criterion reduces to $ka = 1.0$, and the disruption velocity can be approximated by Equation (38) for a low viscosity jet when $G > 100$ and by Equation (40) for a high viscosity jet when $G << 100$. Jet disruption may occur prior to drop merging.

7. Experimental data obtained from thirteen mutually saturated liquid-liquid systems covering a wide range of physical properties show good agreement with theoretical predictions.

8. Experiments were run with wire mesh screens in the nozzle. The major effect of the increase in disturbance level was a decrease in the jet disruption velocity. The decrease was often sufficiently great that abrupt jet lengthening did not occur.

9. Two mass transfer systems were studied. Many of the effects observed can be explained by the effect of solute on the interfacial tension. The direction of mass transfer had an additional effect, transfer out of the jet causing an increase in the disturbance growth rate.

ACKNOWLEDGMENT

The authors acknowledge with thanks the Ford Foundation Fellowship awarded to B. J. Meister. They also express thanks to Dr. J. S. Vrentas of The Dow Chemical Company for his constructive comments and suggestions.

NOTATION

a = jet radius, cm.
a_L = jet radius at end of jet, cm.
a_N = jet radius at nozzle exit, cm.
A, B, C, D = constants in velocity profile equations
c = celerity of wave, cm./sec.
D_F = drop diameter, cm.
D_N = nozzle diameter, cm.
g = acceleration of gravity, 980 cm./sq.sec.
G = $a_N U_N \Delta\rho\mu/\mu'^2$
i = square root of -1
$I_n(ka)$ = modified Bessel function of the first kind of order n
I_{0k} = $I_0(ka)/I_1(ka)$
k = wave number of disturbance, cm.$^{-1}$
ka = dimensionless wave number
K' = constant
$K_n(ka)$ = modified Bessel function of the second kind of order n
K_{0k} = $K_0(ka)/K_1(ka)$
L = jet length, cm.
N_{Re} = dispersed phase Reynolds number, $D_N U_N \rho'/\mu'$
N_{We} = dispersed phase Weber number, $U_N^2 \rho' D_N/\sigma$
Q = volume flow rate of dispersed phase, cc./sec.
r = radial distance, cm.
S = number of axes of symmetry about which perturbation oscillates
t = time, sec.
U_A = average velocity in jet, cm./sec.
U_I = interfacial velocity of jet, cm./sec.
U_J = velocity at which a jet first forms, cm./sec.
U_M = centerline velocity of jet, cm./sec.
U_N = average dispersed phase velocity at nozzle exit, cm./sec.
U_o, U_o' = characteristic velocities of continuous and dispersed phases, cm./sec.
U_{Ri} = average rise velocity of drop over first drop diameter of rise, cm./sec.
$U_{R\infty}$ = steady state rise velocity of drop, cm./sec.
U_z, U_z' = axial velocities of continuous and dispersed phases, respectively, cm./sec.
z = axial distance, cm.

Greek Letters

α = growth rate of disturbance, sec.$^{-1}$
ξ = amplitude of disturbance, cm.
ξ_0 = initial amplitude of disturbance, cm.
μ, μ' = viscosities of continuous and dispersed phases, respectively, g./(cm.)(sec.)
ρ, ρ' = densities of continuous and dispersed phases, respectively, g./cc.
σ = interfacial tension, dyne/cm.
T_{rz} = shear stress, dyne/sq.cm.

LITERATURE CITED

1. Addison, C. C., and T. A. Elliott, *J. Chem. Soc.*, 3096 (1950).
2. Christiansen, R. M., Ph.D. thesis, Univer. Pennsylvania, Philadelphia (1955).
3. Davidson, L., and E. H. Amick, *AIChE J.*, **2**, 337 (1956).
4. Debye, P., and J. Daen, *Phys. Fluids*, **2**, 416 (1959).
5. Fujinawa, K., T. Maruyama, and Y. Nakaike, *Kagaku Kikai*, **21**, 194 (1957).
6. Garner, F. H., P. Mina, and V. G. Jenson, *Trans. Faraday Soc.*, **48**, 1627 (1959).
7. Grant, R. P., and S. Middleman, *AIChE J.*, **12**, 669 (1966).
8. Haenlein, A., *Natl. Advisory Comm. Aeronaut. Tech. Memo No. 659* (1932).
9. Harmarthy, T. Z., *AIChE J.*, **6**, 281 (1960).
10. Hayes, W. B., B. W. Hardy, and C. D. Holland, *ibid.*, **5**, 319 (1959).
11. Hu, S., and R. C. Kintner, *ibid.*, **1**, 42 (1955).
12. Keith, F. W., and A. N. Hixson, *Ind. Eng. Chem.*, **47**, 258 (1955).
13. Klee, A. J., and R. E. Treybal, *AIChE J.*, **2**, 244 (1956).
14. Levich, V. G., "Physicochemical Hydrodynamics," Prentice Hall, New York (1962).
15. Meister, B. J., Ph.D. thesis, Cornell Univer., Ithaca, N. Y. (1966).
16. ———, and G. F. Scheele, *AIChE J.*, **13**, 682 (1967).
17. Merrington, A. C., and E. G. Richardson, *Proc. Phys. Soc.*, **59**, 1 (1947).
18. Ohnesorge, G., *Z. angew Math. Mech.*, **16**, 355 (1936).
19. Ranz, W. E., *Can. J. Chem. Eng.*, **36**, 175 (1958).
20. ———, and W. M. Dreier, *Ind. Eng. Chem. Fundamentals*, **3**, 53 (1964).
21. Rayleigh, Lord, *Proc. Royal Soc.*, **29**, 71 (1879).
22. Scheele, G. F., and B. J. Meister, *AIChE J.*, **14**, 9, 15 (1968).
23. Scriven, L. E., and R. L. Pigford, *ibid.*, **5**, 397 (1959).
24. Shiffler, D. A., Ph.D. thesis, Cornell Univer., Ithaca, N. Y. (1965).
25. Siemes, W., and J. F. Kauffmann, *Chem. Ingr. Tech.*, **29**, 32 (1957).
26. Smith, S. W. J., and H. Moss, *Proc. Royal Soc.*, **A-93**, 373 (1917).
27. Taylor, G. I., "The Scientific Papers of Sir Geoffrey Ingram Taylor," Vol. 3, No. 25, Cambridge, Eng. (1963).
28. Tomotika, S., *Proc. Royal Soc.*, **A150**, 322 (1935).
29. Tyler, E., and E. G. Richardson, *Proc. Phys. Soc.*, **37**, 297 (1925).
30. ———, and F. Watkin, *Phil. Magazine*, **14**, 849 (1932).
31. Vandegrift, A. E., Ph.D. thesis, Univer. California, Berkeley (1963).
32. Vrentas, J. S., and J. L. Duda, *Chem. Eng. Sci.*, **22**, 855 (1967).
33. Weber, C., *Z. angew Math. Mech.*, **11**, 136 (1931).
34. Ziabicki, A., and R. Takserman-Krozer, *Roczniki Chemii*, **37**, 1607 (1963).

Manuscript received August 2, 1967; revision received May 13, 1968; paper accepted May 20, 1968.